Hindawi
Geofluids
Volume 2022, Article ID 1149000, 12 pages
https://doi.org/10.1155/2022/1149000

Research Article

Study on Mechanism and Control Technology of Asymmetric Floor Heave in a Deep Soft Rock Main Roadway

Fulian He,[1,2] Wenli Zhai,[1] Xuhui Xu,[1] Jiayu Song,[1] Liang Li,[1] and Kai Lv[1]

[1]*School of Energy & Mining Engineering, China University of Mining & Technology (Beijing), Beijing 100083, China*
[2]*Beijing Key Laboratory for Precise Mining of Intergrown Energy and Resources, China University of Mining & Technology (Beijing), Beijing 100083, China*

Correspondence should be addressed to Wenli Zhai; wlzhai8@163.com

Received 26 April 2022; Revised 20 June 2022; Accepted 7 July 2022; Published 23 July 2022

Academic Editor: Dongjiang Pan

Considering the serious asymmetric deformation and failure of the floor of 1# main roadway in Wanglou Coal Mine, the mechanism of roadway asymmetric floor heave was studied through on-site investigation, theoretical analysis, numerical simulation, and on-site test. The following conclusions were drawn: (1) the floor heave of 1# main roadway is mainly caused by high original rock stress, surrounding rock stress, water physical effect, support strength, etc. (2) A mechanical model of asymmetric floor heave is built and analyzed. Roadway floor stability is relevant to the stress concentration coefficient of the roadway sides, the burial depth of the roadway, and the cohesion and internal angle of friction of the floor rock. The relationship between the upward resultant force of the floor and the stress concentration coefficient of the roadway sides is established. Affected by mining, the upward force of roadway floor reaches 17.0 MPa, and serious floor heave is easy to occur when the floor is opened. (3) The floor heave curve of the position of 1# main roadway corresponding to working face is obviously asymmetric, the maximum value of floor heave being 948 mm. The floor heave curve of other positions of 1# main roadway is basically symmetric, the maximum floor heave value being merely 497 mm. A new "differentiated" combined support is proposed and field tested. It has been 13 months since the completion of main roadway repair in this section, no obvious deformation occurred, and the long-term stability of soft rock roadway support in deep mines is realized.

1. Introduction

With the gradual depletion of shallow coal resources, coal mining in China is advancing to an increasingly deep level year by year. Deep mining will be quite common in the development of coal resources [1–4]. The surrounding rock of deep roadway is subject to not only high ground stress but also the mining during excavation and recovery [5]. This effect often leads to asymmetric failure, especially the floor heave, which makes the repair more difficult and frequent. This leads to higher requirements for the control of deep roadway surrounding rock; that is, single support cannot control large deformation of deep roadway surrounding rock [6–9]. According to the different action mechanism of the support in the control process, there are mainly reinforcement method, pressure relief method, combined support method, and so on [10–14].

Scholars at home and abroad have conducted extensive research on the surrounding rock control of deep roadway and the mechanism of roadway floor heave. Through quantities of on-site engineering practice, Wang et al. [15] summarized two common repair schemes: (1) grouting reinforcement to improve the strength and integrity of rock mass and (2) high-strength support components to improve the support resistance of the support system. Mo et al. [16] introduced a new floor classification system, the coal mine floor rating, based on the underlying failure mechanisms. M. Wang et al. [17]. Based on a case study of a longwall entry employing a stiff-yield pillar configuration, massive floor heave occurs at the entry rib that takes less loads and eventually propagates towards the other rib bearing a significant amount of loads. Hou [18] conducted rock mechanics experiments and proved that under the action of high ground stress, the brittle failure of rock in deep roadway

changed to ductile rheological failure, accompanied by large plastic deformation; he also put forward a technical concept of "two supports." Guo et al. [19] used theoretical analysis and numerical analysis methods to analyze the failure characteristics of floor surrounding rock and put forward the flexural instability criterion of floor. With respect to floor heave control, Kang [20] believed that floor heave was caused by the following three aspects: the buckling of unstable floor strata into the roadway, the expansion under the action of eccentric stress, and the water-induced rock swelling. Yang et al. [21] studied the mechanism of floor heave in soft rock roadway and proposed a new coupling support technology of a bolt-mesh-anchor-base angle bolt-flexible layer truss for controlling the floor heave of roadway. Xu and Wei [22] used the finite element method to analyze the stress environment and failure mechanism of the surrounding rock of the soft rock roadway floor under the superposition of high stress and mining stress and proposed the joint control technology to effectively control the occurrence of roadway floor heave. Wen et al. [23] analyzed the mechanism of floor heave in soft rock roadway and put forward an inverted floor arch control technology characterized by pressure relief and reinforcement. Z. Wang et al. [24] analyzed the characteristics of asymmetric floor heave along the goaf. Sun [25] studied the control of roadway floor heave by roadway grooving and pressure relief. Chen et al. [26] evaluated the damage degree of floor heave under different conditions, statistically analyzed the main evaluation indexes of roadway floor heave damage degree, and verified the rationality and accuracy of this method through the field measured values and evaluation values. Sun et al. [27] studied the floor heave and failure through the comprehensive analysis of the collected infrared images and video photos and changes of strain field; the research results show that the horizontal stress has a great impact on the floor heave.

According to the mine data, 1# roadway floor is seriously damaged and has been repaired for many times. The average repair cycle is about 6 months, and the thickness of each bottom is about 0.5 m, as shown in Figure 1, which seriously affects the normal use of the roadway. Therefore, the asymmetric failure mechanism of roadway floor is studied by means of theoretical analysis and numerical simulation, combined with field test and other methods [28]. Furthermore, a "differentiated support" scheme was proposed; different positions adopt different support methods: anchor mesh cable shotcrete+inverted floor arch+grouting+closed O-shaped steel shed, and anchor mesh cable shotcrete +inverted floor arch+grouting. This support technology ensures the safe and stable support of the main roadway.

2. Engineering Background

2.1. Project Profile. The 1# main roadway in Wanglou Coal Mine mainly serves the second mining area and the deep seventh mining area, and the layout is shown in Figure 2. As both a pedestrian passage and a ventilation, it has a long service life, with a total length of 1,500 m and a buried depth of about 700~930 m. The histogram of coal and rock strata in this area is shown in Figure 3. The roadway in this test section is located in the 1# main roadway between 12302 and 12304 working faces for research. The right side of this section is 49 m away from the goaf, and the left side is 38 m away from the 2# main roadway. According to the mine data, this section has been repaired for many times due to the serious damage of the floor.

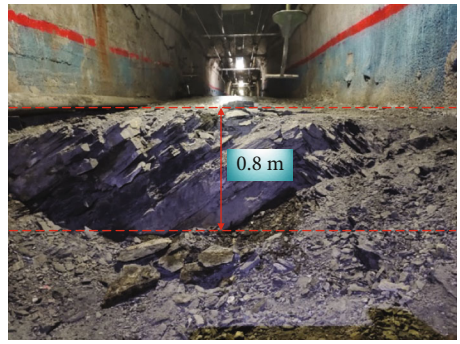

Figure 1: Failure of roadway floor.

2.2. Original Support Scheme and Failure Characteristics. The 1# main roadway has a net width of 3,800 mm, a wall height of 1,500 mm, and an arch height of 1,900 mm. During excavation, the main roadway is supported by resin anchor bolts with equal strength (Φ 20 × 2,500 mm) and row spacing 800 × 800 mm. Anchor cable adopts low relaxation steel strand (Φ 18 × 8,000 mm), and a group of anchor cables are arranged along the roadway center line to both sides, with a spacing of 2 m and a row spacing of 3 m. Metal mesh uses longitude and latitude meshes (150 mm × 100 mm) made of Φ 6 mm reinforced steel bar; the main roadway surface is sprayed with C20 concrete, and the shotcrete layer is 120 mm thick. With the above support scheme, the 1# main roadway mainly exhibits the following deformation and failure characteristics in the section of the 12302-12304 working faces.

(1) The bolts in the 1# main roadway section correspond to the 12302 and 12304 working faces break. The phenomenon mainly occurs in the left rib of the roadway, and the bolt failure mainly belongs to tensile shear failure; it is shown in Figure 4(a)

(2) The 1# main roadway section corresponding to the 12302 and 12304 working faces deforms seriously, which is mainly manifested in roof subsidence, serious cracking of the shotcrete layer, and large overall rib-to-rib displacement, especially serious floor heave. As shown in Figures 4(b), 4(c), and 4(d), deformation is asymmetric

(3) The 1# main roadway undergoes continuous and serious floor heave. The 1# main roadway has been repaired multiple times. Each repair requires quantities of bottom lifting with a short repair cycle of about 6 months, which seriously affects the normal roadway operation

2.3. Cause Analysis of Roadway Failure. Based on comprehensive data and on-site failure characteristics, the floor

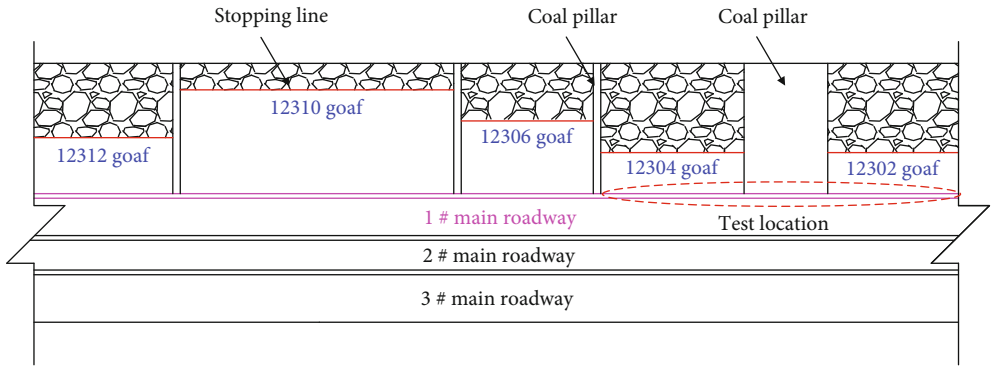

Figure 2: Location of 1# main roadway.

Histogram	Rock stratum	Thickness/m	Lithology description
	Medium sandstone	2.7 ~ 5.6 / 3.2	Light gray, gray, mainly composed of quartz and feldspar, f = 4 ~ 5
	Mudstone	0.7 ~ 1.8 / 1.2	Dark gray, rich in plant fossils, f = 2 ~ 3
	Fine sandstone	6.2 ~ 8 / 7.7	Light gray, mainly composed of quartz, f = 4 ~ 5
	Mudstone	0 ~ 9.2 / 4.5	Dark gray, rich in plant fossils, f = 2 ~ 3
	No.3 coal seam	0 .9 ~ 4 / 1.9	Mainly bright coal, followed by dark coal, asphalt luster, f = 2.3 ~ 3.1
	Mudstone	2.6 ~ 5.9 / 4.0	Dark gray, rich in plant fossils, f = 2 ~ 3
	Siltstone	29 ~ 42 / 37	Gray, dense block, developed horizontal bedding, f = 4 ~ 5

Figure 3: Coal and rock strata histogram.

heave of 1# main roadway is mainly caused by high original rock stress, surrounding rock stress, water physical effect, support strength, etc.

(1) Original Rock Stress. After the buried depth of the roadway increases, the values of roof subsidence and floor heave grow continuously, but the floor heave value grows faster than the roof subsidence value. When the roadway ground stress reaches a certain value, the roadway floor will be damaged. The greater the original rock stress of the roadway is, the more serious the floor heave is [29]. The buried depth of 1# main roadway in the section of the 12302-12304 working faces is 810-850 m, and the surrounding rock of roadway deforms in all directions, floor heave being particularly serious

(2) Surrounding Rock Stress. The 1# main roadway is located within the influence range of front abutment pressure of the 12302 and 12304 working faces. The vertical stress acts on the two ribs to squeeze the floor, resulting in extrusion flow. The floor is where the stress is released and deformation of the roadway occurs, so that it heaves. Moreover, the 1# main roadway has been repaired multiple times, and the loose circle continues to expand after the surrounding rock is broken, which accelerates the roadway deformation

(3) Water Physical Effect. The 1# main roadway is located in coal seams, and its floor is mainly argillaceous. Affected by the water in the shallow goaf, it has a low floor strength and is more prone to failure [30]

(4) Support Strength. The original support of the roadway is ordinary support, and the floor is in an unsupported state. Under this condition, the floor with a low bearing capacity is where roadway stress is released and deformation occurs, and the floor is likely to heave

3. Mechanical Model of Roadway Floor Heave

The 1# main roadway is arranged within the influence range of front abutment pressure and is damaged to varying

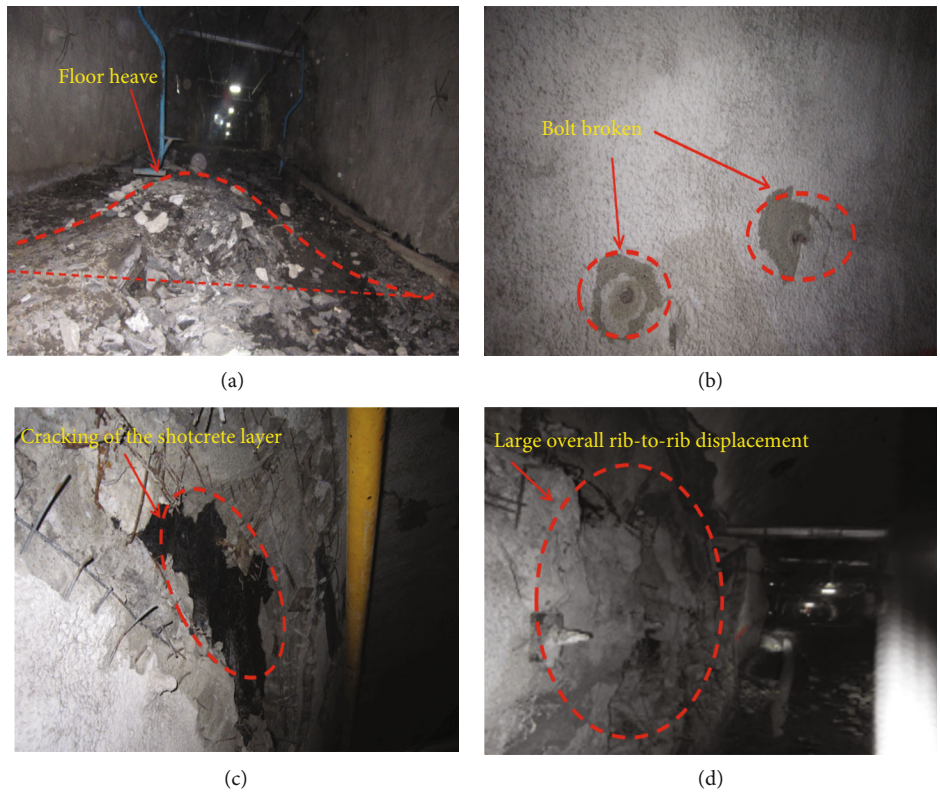

Figure 4: Deformation and failure of 1# main roadway. (a) Bolt broken. (b) Cracking of the shotcrete layer. (c) Large overall rib-to-rib displacement. (d) Floor heave.

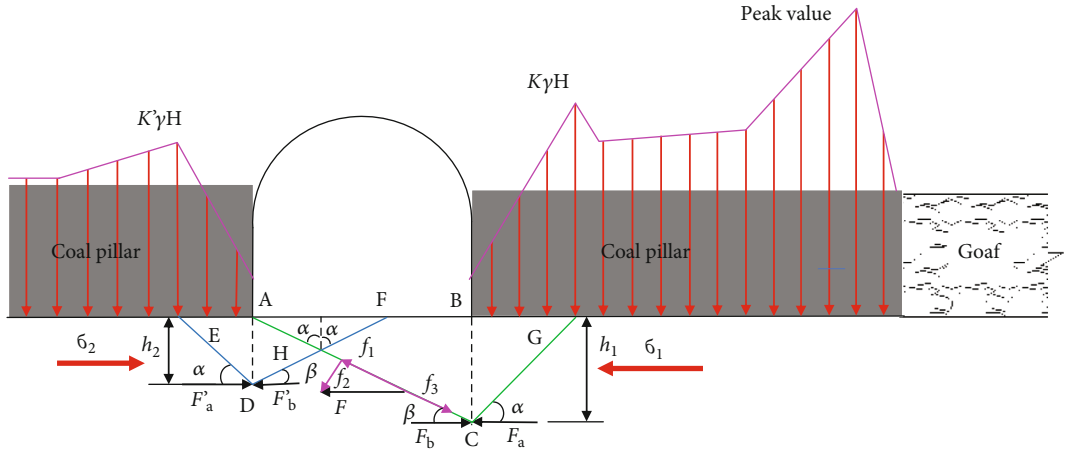

Figure 5: Mechanical model of floor heave.

degrees under the influence of high ground stress [31]. Considering the above fact, with reference to the Rankine pressure theory [32], it is assumed that the floor is cohesive soil and is in the limit equilibrium state. Under this assumption, a mechanical model of roadway floor heave within the influence range of front abutment pressure is established, as shown in Figure 5.

To facilitate the calculation, according to the elastic-plastic theory, the stress distribution of the uniformly distributed load on the semi-infinite plane in the floor differs slightly from that of the triangular load and trapezoidal load (with the same average value) in the floor. On the premise of meeting the accuracy requirements of mining engineering, the range of floor stress increase area caused by both ribs of the roadway can be represented by the average vertical stress $(K+1)\gamma H/2$ and $(K'+1)\gamma H/2$, respectively, where K and K' are the vertical stress concentration coefficients of the two ribs of the roadway. Both sides of the roadway are influenced by the front abutment pressure, and the critical depths of rock mass movement of the right

and left rib floor are h_1 and h_2, respectably. Under the action of vertical stress, the roadway floor rock mass forms an active pressure zone BCG and a passive pressure zone ABC, with BC serving as the "retaining wall." These two zones squeeze the "retaining wall" BC. Besides, the active pressure area ADE and the passive pressure area ADF are formed, with AD serving as the "retaining wall." These two zones squeeze the "retaining wall" AD. Moreover, both sides of the roadway are also affected by the horizontal stress σ_1 and σ_2. As a result, the rock mass in the active pressure areas BCG and ADE is in an active plastic sliding state, while that in the passive pressure areas ADF and ABC is in a passive plastic sliding state due to the extrusion of both sides. Since there is no space for rock mass movement below CDH, the roadway floor is not supported during excavation, and it is in an "open" state. When the pressure exceeds the ultimate strength that the rock mass of the roadway floor can bear, the roadway floor will lift up, resulting in floor heave [33].

When the floor rock mass is in the Rankine limit equilibrium state, with the floor rock mass on the right side of the roadway as an example, the Rankine active slip angle $\alpha = 45^\circ - \varphi/2$; Rankine passive slip angle $\beta = 45^\circ + \varphi/2$, where φ is the friction angle in the rock mass, and the force acting on point C is

$$\begin{aligned} F_a &= \left(\gamma h_1 + \frac{K+1}{2}\gamma H\right)\tan^2\alpha - 2c\tan\alpha, \\ F_b &= \gamma h_1 \tan^2\beta - 2c\tan\beta, \end{aligned} \tag{1}$$

where γ is the gravity density of strata, kN/m^3; H is the depth of coal seam, m; K is the stress concentration coefficient; and c is cohesion.

When the active pressure F_a acting on the critical interface BC is greater than the passive pressure F_b, the critical interface BC is squeezed and affected by horizontal stress σ_1. The resultant force F of F_a, F_b, and σ_1 will be the force source of ABC rock mass movement:

$$\begin{aligned} F &= F_a - F_b + \sigma_1 \\ &= \gamma h_1\left(\tan^2\alpha - \tan^2\beta\right) + \frac{K+1}{2}\gamma H\tan^2\alpha \\ &\quad - 2c(\tan\alpha - \tan\beta) + \sigma_1. \end{aligned} \tag{2}$$

The resultant force F is decomposed along the AC plane as f_1, and the component forces perpendicular to the AC plane are f_2, f_1, and f_2, respectively.

$$\begin{aligned} f_1 &= F\sin\alpha, \\ f_2 &= F\sin\beta. \end{aligned} \tag{3}$$

During rock mass movement, friction f_3 will be generated on the AC surface due to the pressure f_2 perpendicular to the AC surface.

$$f_3 = F\sin\beta\tan\varphi. \tag{4}$$

The resultant force S on the AC plane is

$$S = f_1 - f_3 = F(\sin\alpha - \sin\beta\tan\varphi). \tag{5}$$

Similarly, the resultant force S' along DF plane on the left side of the roadway is

$$S' = F'(\sin\alpha - \sin\beta\tan\varphi), \tag{6}$$

$$\begin{aligned} F' &= \gamma h_2\left(\tan^2\alpha - \tan^2\beta\right) + \frac{K'+1}{2}\gamma H\tan^2\alpha \\ &\quad - 2c(\tan\alpha - \tan\beta) + \sigma_2. \end{aligned} \tag{7}$$

According to Equations (2) and (7), the thrusts on both sides of the roadway differ obviously. Under the same internal friction angle, the thrusts on both sides of the roadway are correlated to the horizontal stress, the stress concentration coefficient on both sides of the roadway, and the critical depth of floor rock mass movement on both sides of the roadway. As the roadway is affected by the front abutment pressure during working face recovery, both sides of the roadway correspond to different stress concentration coefficients; this is the main reason for the roadway floor heave. The force source of floor heave is the resultant force R of the force S along the AC plane and the force S' along the DF plane.

$$R = S\cos\alpha + S'\cos\alpha. \tag{8}$$

It can be seen from the above formula that the stability of the roadway floor is related to the stress concentration factor of the two sides of the roadway, the buried depth of the roadway, the cohesion of the floor rock mass, and the internal friction angle.

According to the geological conditions of the mine, the buried depth of 1# main roadway is taken as 800 m, $\gamma = 25$ kN/m3, $\varphi = 21^\circ$, and $C = 1.1$ MPa; assuming $h_1 = 3.0$ m and $h_2 = 2.5$ m, the ratio of horizontal stress to vertical stress is 1.2, $\sigma_1 = \sigma_2 = 1.2\,\gamma H$. Thus, the variation of the resultant force R upward of the roadway floor with the stress concentration factors K and K' on both sides of the roadway can be calculated as follows:

$$R = 13.7 + 1.1\left(K + K'\right). \tag{9}$$

Draw the variation curve of resultant force R with K and K', as shown in Figure 6. When the roadway is outside the influence range of advance bearing pressure, such as$K = K' = 1.2$and$R = 16.34$ MPa, and when the roadway enters the influence range of advance bearing pressure, the stress concentration degree on both sides is different,$K > K'$, such as$K = 1.6, K' = 1.4$, and$R = 17.0$ MPa, indicating that affected by mining, there is a large gap in stress concentration on both sides of the roadway, reaching 17.0 MPa; when the floor is open, serious floor heave is easy to occur, so in order to effectively reduce the impact of roadway floor heave on

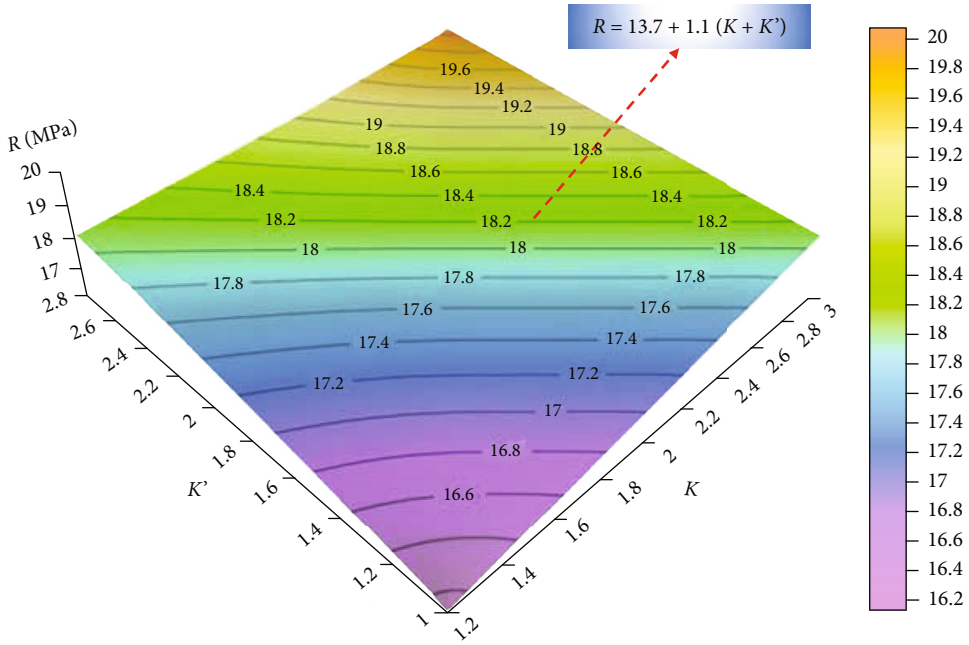

Figure 6: Variation curve of R with K and K'.

safety production, the strength of floor support needs to be strengthened.

4. Numerical Simulation Analysis

According to the geological data of Wanglou Coal Mine, 1# the main roadway is connected by the connecting roadway between 12302 and 12304 working faces. It buried in the coal seam at a depth of 810-850 m. The stopping line of the 12302 and 12304 working faces is 49 m away from 1# main roadway. A numerical model was established by FLAC3D simulation software, as shown in Figure 7. The model is 150 m long, 210 m wide, and 90 m high. A vertical stress of 19.5 MPa was applied to the upper surface of the model. The failure criterion of rock strata was simulated by the Mohr-Coulomb model. The side of the model is limited in the horizontal displacement, and the bottom was fixed in X, Y, and Z directions to simulate the gravity load of overlying rock. The mechanical parameters of coal and rock mass are shown in Table 1.

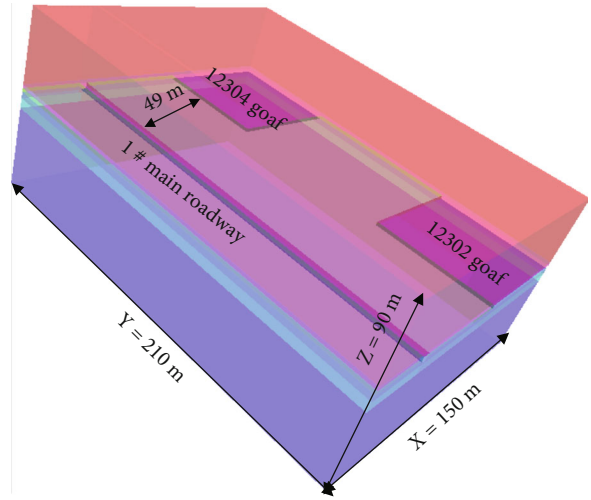

Figure 7: Numerical model.

With reference to the three-dimensional ground stress field test report of Wanglou Coal Mine, when the buried depth is 830 m, the vertical stress is 22.1 MPa. The front abutment pressure curve is drawn by the detection of the front abutment pressure, as shown in Figure 8. The peak value of the front abutment pressure is about 6 m away from the working face; the maximum value is 61.9 MPa; the stress concentration coefficient is about 2.80, and the influence range of the front abutment pressure reaches around 78 m. The peak values of vertical stress on the left and right sides of 1# roadway are 33.6 MPa and 30.8 MPa, respectively, and the stress concentration coefficients are 1.52 and 1.39, respectively. Affected by the front abutment pressure, the maximum vertical stress on the right side of roadway is 2.8 MPa higher than that on the left side.

The position in the 1# main roadway corresponding to the 12302 working face is affected by the front abutment pressure of the recovery working face, as shown in Figure 9; the support pressure of the surrounding rock on both sides of the roadway is distributed asymmetrically. The stress concentration degree and range of the surrounding rock on the side of the recovery working face are larger than those on the other side; this is consistent with the early-established mechanical model of floor heave caused by the front abutment pressure. Furthermore, it can be seen from the stress nephogram that the stress of the roadway

Table 1: Mechanical parameters of coal and rock.

Lithology	ρ (kg/m^3)	E_i (GPa)	c_i (MPa)	φ_i (deg.)	σ_{ci} (MPa)	σ_{ti} (MPa)	ν_i
Medium sandstone	2795	8.26	6.17	37.28	55.69	1.43	0.31
Siltstone	2612	6.52	5.25	32.24	45.76	1.26	0.25
Fine sandstone	2480	6.36	5.94	33.37	32.53	1.56	0.25
Mudstone	1820	4.53	2.80	22.25	20.15	1.33	0.08
Coal	1525	3.76	1.13	19.68	23.32	1.61	0.23

ribs is more concentrated than that of the roof surrounding rock, and the maximum stress concentration coefficient is about 1.6.

As can be seen from Figures 10 and 11, the stopping line of the 12302 and 12304 working faces is 49 m away from 1# main roadway. After the recovery of the two working faces, the horizontal stress of the position in 1# main roadway corresponding to the two working faces is greater than that corresponding to the coal pillars between the two working faces. According to the position where $Y = 30$ m, the horizontal stress difference on both sides of the roadway is 2.5 MPa, which also displays obvious asymmetry.

Through the detection of roadway floor heave at the positions where $Y = 30$ m and $Y = 100$ m, as can be seen from Figure 12, the floor heave curve of 1# main roadway corresponding to 12302 working face ($Y = 30$ m) is an obvious asymmetric one; the maximum floor heave is 948 mm. Overall, roadway floor undergoes serious failure; the failure depth reaches 7 m. The displacement values of roadway floor below 7 m are negative values, and the roadway is overall squeezed. The floor heave curve of 1# main roadway corresponding to the coal pillars ($Y = 100$ m) is basically symmetric, and the maximum floor heave is 497 mm. The floor heave value of the roadway at the position where $Y = 30$ m is significantly greater than that at the position where $Y = 100$ m.

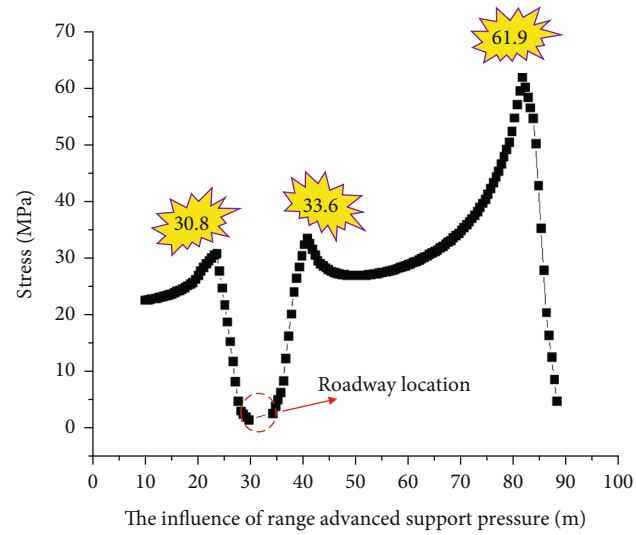

Figure 8: Advance abutment pressure curve.

5. Design of Repair Support Scheme

Therefore, the design of support scheme should take targeted support for the roadway floor to overcome the force source of floor heave in the roadway and improve the supporting capacity of surrounding rock. Meanwhile, the roadway shows obvious asymmetric failure due to the influence of front abutment pressure and horizontal stress. In addition, the support strength of the right rib of the roadway shall be properly strengthened to avoid the roadway failure caused by asymmetric force source. Therefore, a final "differentiated support" was determined. For the position of 1# main roadway corresponding to the goaf of the 12302 and 12304 working faces, a combined support of anchor mesh cable shotcrete+inverted floor arch+grouting+closed O-shaped steel shed is adopted; the position of 1# main roadway corresponding to coal pillars adopts anchor mesh cable shotcrete+inverted floor arch+grouting support.

5.1. Support Scheme for Roadway Roof and Ribs. After the main roadway expands to the design section, the full section anchor mesh cable support shall be adopted, as shown in Figure 13. Anchor bolt uses high-strength preload anchor bolt (Φ 22 × 2,800 mm, torque 350 N·m); anchor cable uses mine common anchor cable (Φ 21.6 × 8,000 mm, preload no less than 30 MPa); metal mesh adopts welded longitude and latitude mesh (100 × 100 mm meshes) of Φ 6 mm reinforced steel bar; anchor bolt tray is high-strength arc tray (150 × 150 × 10 mm), and steel belt guard plate (450 × 280 × 3.75 mm) and anchor cable tray use high-strength arc tray (300 × 300 × 16 mm). Furthermore, to balance the roadway failure caused by asymmetric force sources on both sides of the roadway, the upper rib and footings on the right side of the roadway are supplemented with mine common anchor cable (Φ 21.6 × 5,000 mm).

5.2. Inverted Floor Arch Support and Grouting Reinforcement Scheme

(1) Inverted Floor Arch Anchor Bolt Construction. High-strength preload anchor bolt (Φ 22 × 2,800 mm) coordinates anchor bolt disc (200 × 200 × 10 mm) to strengthen the support, and the row spacing between anchor bolts is 800 × 800 mm, anchor bolt preload 350 N·m; metal mesh (80 × 80 mm meshes) made of Φ 6 mm steel is adopted

(2) Grouting. The grouting pipe (Φ 20 × 2,000 mm) is processed by seamless steel pipes (diameter 12.7 mm and wall thickness 3 mm). To facilitate the process,

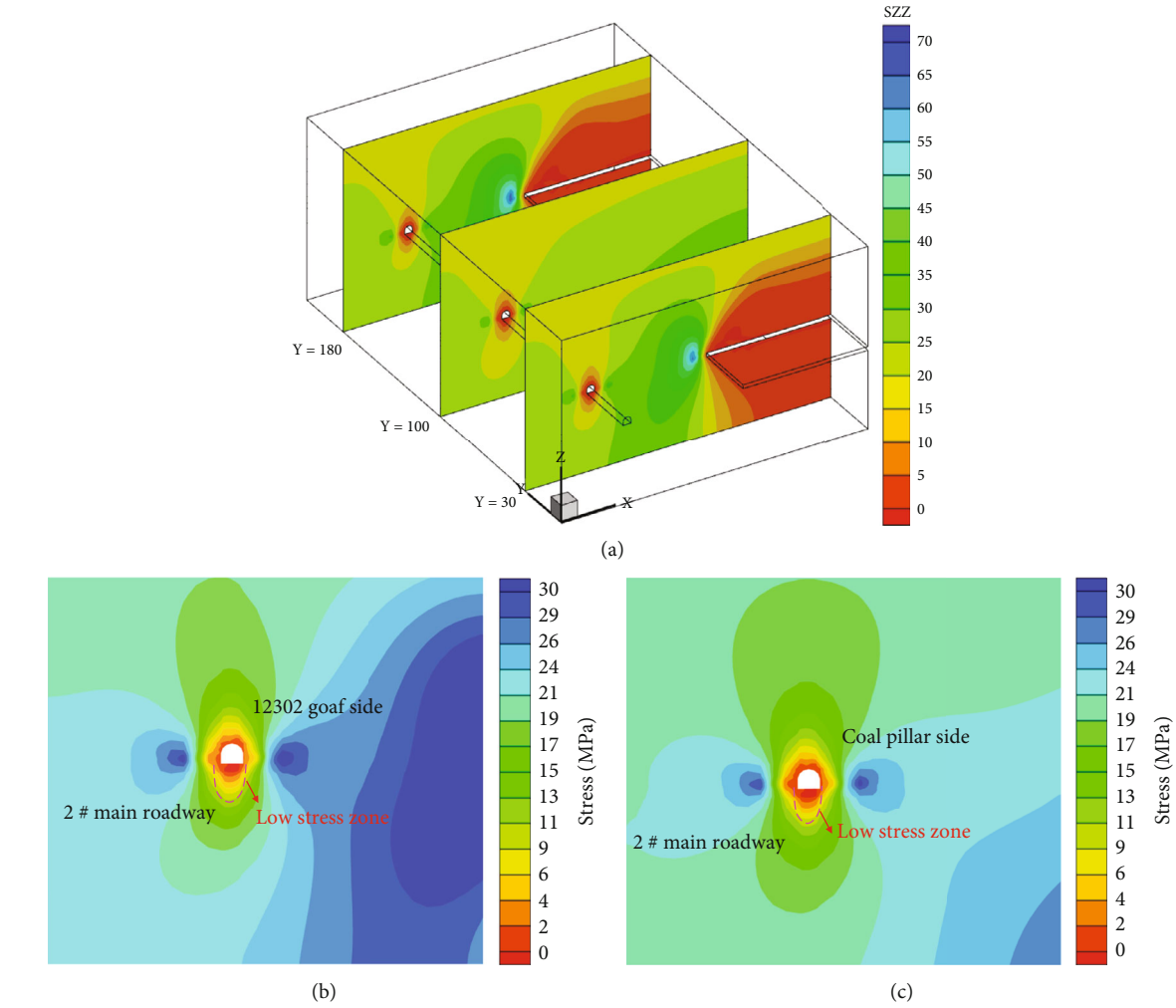

Figure 9: Vertical stress distribution. (a) Stress distribution at different positions of roadway. (b) $Y = 30$. (c) $Y = 100$.

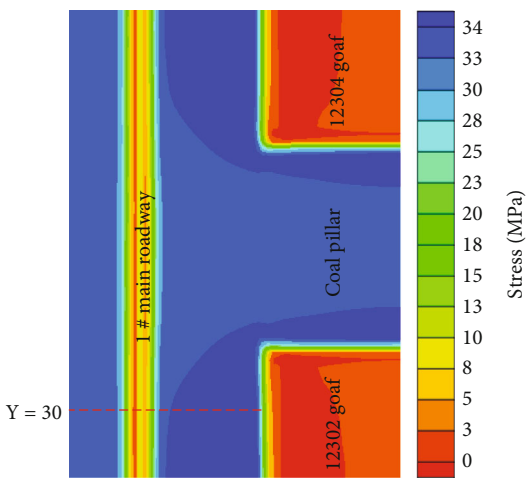

Figure 10: Horizontal stress distribution.

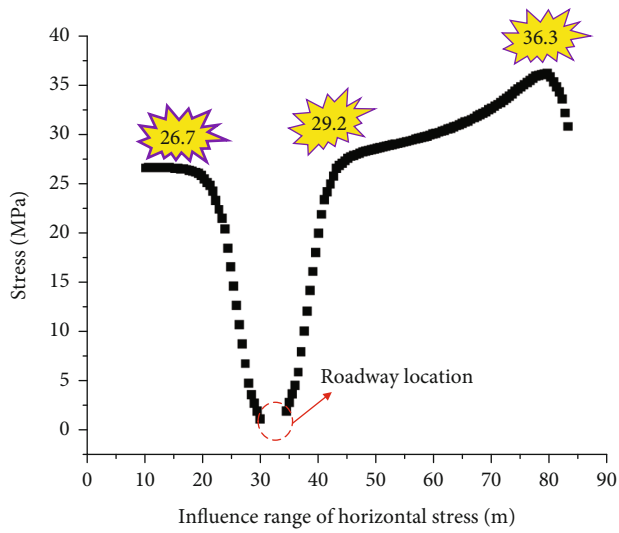

Figure 11: Horizontal stress curve at $Y = 30$.

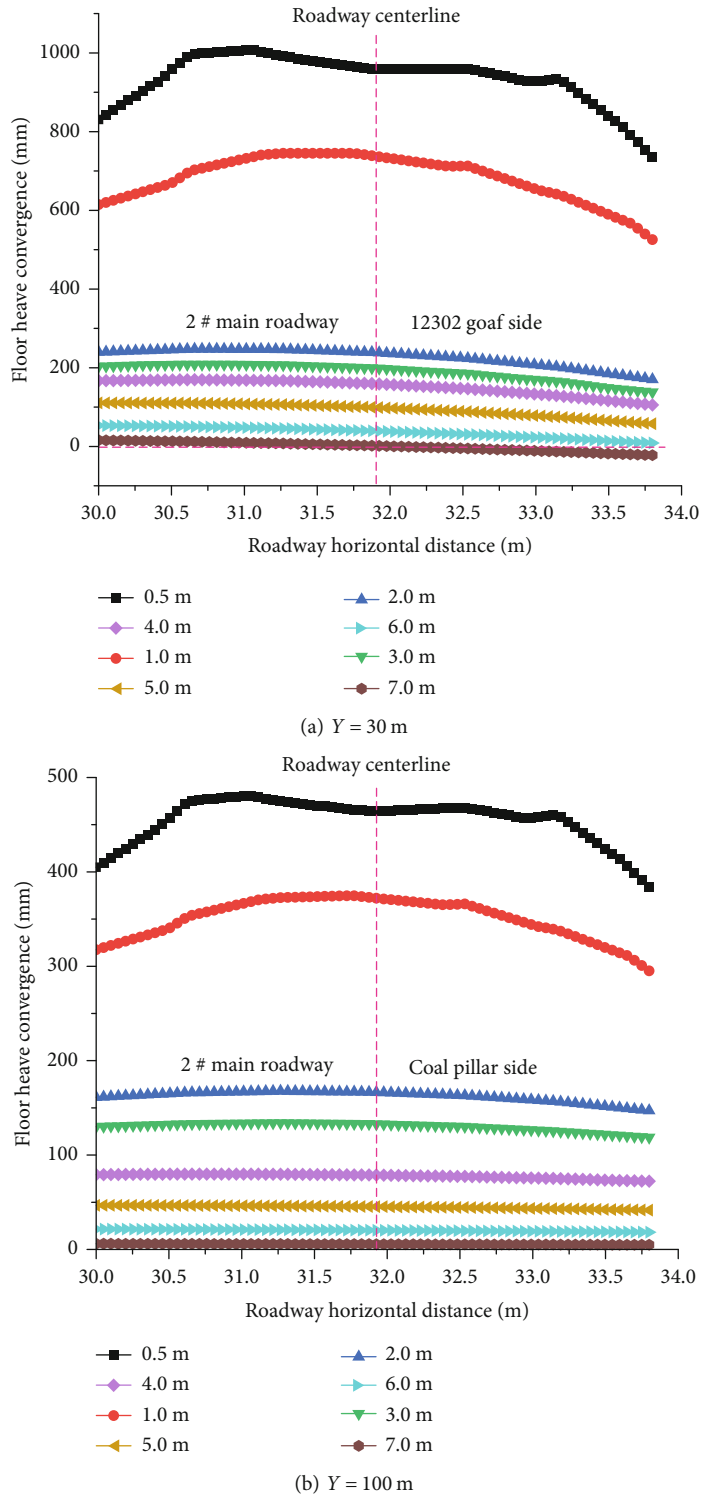

Figure 12: Floor heave curve.

short grouting pipes (Φ 20 × 1,000 mm) are prepared for use when the roadway is extremely broken

Initial grouting process: floor reshaping into an arch→-construction of grouting borehole and the installation of grouting pipes on the floor→grouting reinforcement on the floor, as can be seen from Figures 13(a) and 13(b). First, grouting pipes (Φ 20 × 2,000 mm) are arranged at a row spacing of 1,600 mm and a spacing of 1,600 mm, as shown in Figure 14. During pipe grouting, if the main roadway is quite broken locally, making it difficult to form holes, short grouting pipes (Φ 20 × 1,000 mm) are adopted and grouting pipes (Φ 20 × 2,000 mm) are densely arranged. The pipe grouting shall be completed at one time, and the holes shall

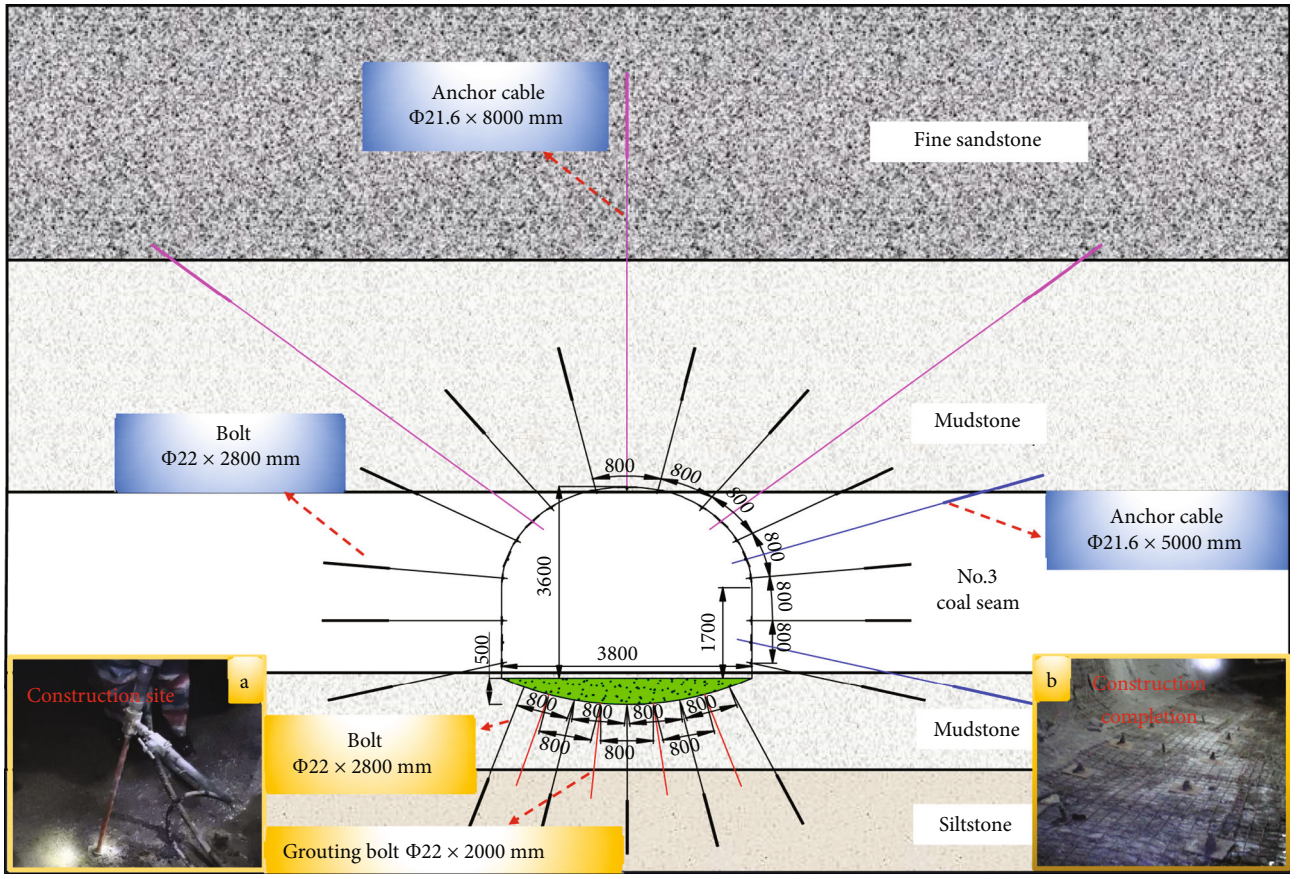

Figure 13: Section support scheme.

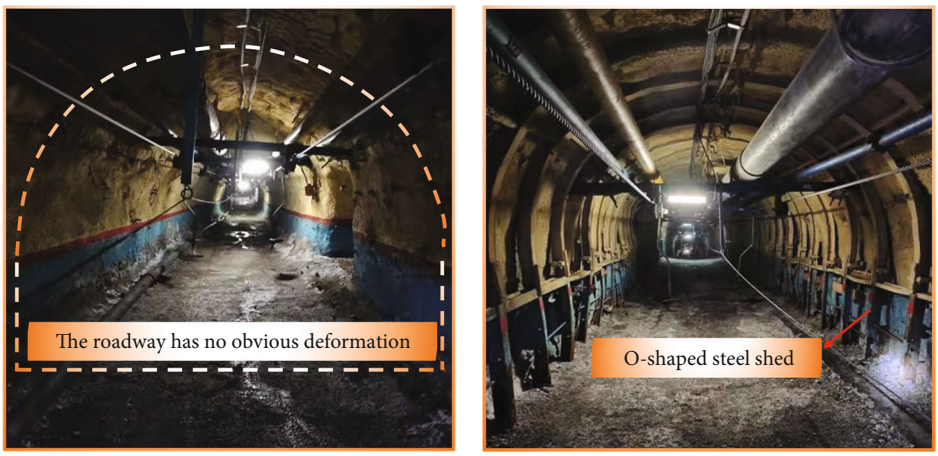

(a) (b)

Figure 14: Field support effect. (a) Reinforced support section. (b) Ordinary support section.

be sealed on time upon the completion of construction of each grouting pipe.

Grouting shall be conducted from the lower end to the upper end (or section by section) of 1# main roadway. The grouting sequence is from the middle to both sides. During grouting, when the final grouting pressure of the grouting pipe is 3.0 MPa, a ball valve is used to seal the hole in time. In the case of slurry leakage, cement is adopted for plugging in time. If slurry leakage occurs in adjacent grouting pipe holes, a ball valve is installed for plugging. If the slurry leakage area is too large to be plugged, grouting stops for half an hour, during which other grouting pipes are grouted first.

5.3. Reinforcement Support Scheme of Closed O-Shaped Steel Shed. As 1# main roadway is affected by high ground stress and front abutment pressure, "closed O-shaped" steel shed

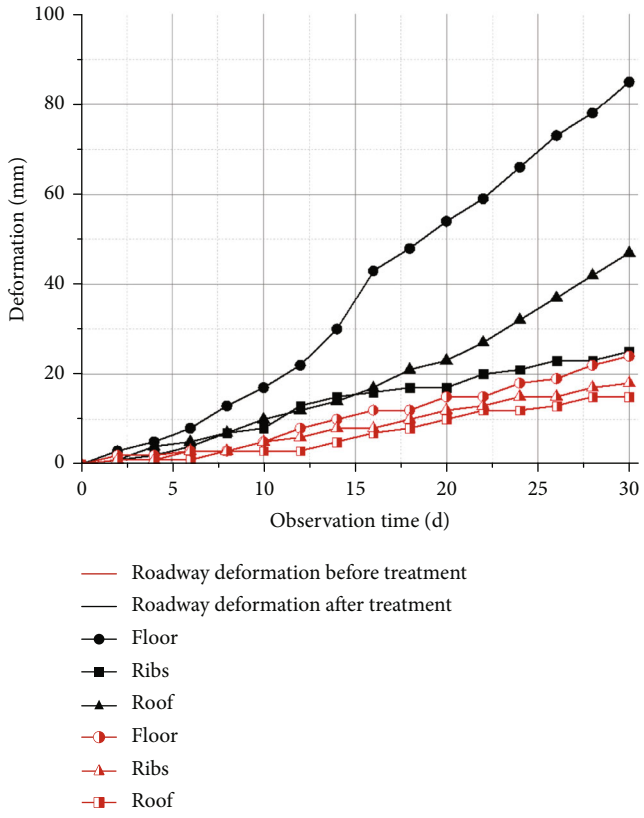

Figure 15: Monitoring curve of engineering practice.

is used to reinforce and support the position of 1# main roadway corresponding to the 12302 and 12304 working faces. The closed O-shaped steel shed is processed by 11# H-shaped steel. The steel shed falls into four sections (arch section, left rib section, right rib section, and floor section). The components are processed by 20 mm thick steel plates. The support spacing of the steel shed is 0.8 m. The two groups of steel sheds are connected and fixed by five 22 kg rails.

Full section shotcreting is carried out for the repaired roadway, with a concrete spraying thickness of 50 mm. After shotcreting, the upper part of the inverted floor arch is backfilled with crushed gangue.

6. Examination of Experimental Effect

Five groups of ground pressure observation points were arranged in the test section of 1# roadway, and continuous monitoring for one month, the results are shown in Figure 15; the results show that before roadway treatment the inner floor heave, the rib-to-rib displacement and the roof subsidence are 85 mm, 47 mm, and 25 mm, respectively. After adopting the combined support of anchor mesh cable shotcrete+inverted floor arch+grouting+closed O-shaped steel shed, the three values fall to 24 mm, 18 mm, and 15 mm, respectively (these data are the average values of each measuring point of the test section in the main roadway); the overall deformation of the roadway is greatly reduced, especially the deformation of the roadway floor. Hence, this support scheme effectively realizes the stable support of soft rock roadway in deep mines. The field support effect is shown in Figure 14.

7. Conclusions

(1) The floor heave of 1# main roadway is mainly caused by high original rock stress, surrounding rock stress, water physical effect, support strength, etc.

(2) A mechanical model of asymmetric floor heave is built and analyzed. Roadway floor stability is relevant to the stress concentration coefficient of the roadway sides, the burial depth of the roadway, and the cohesion and internal angle of friction of the floor rock. The relationship between the upward resultant force of the floor and the stress concentration coefficient of the roadway sides is established

(3) At the floor of 1# main roadway corresponding to the mining working face, the maximum floor heave is 948 mm. At the position of 1# main roadway corresponding to the coal pillars, the maximum floor heave is just 497 mm. Meanwhile, the stress of the two ribs of the main roadway is more concentrated than that of the roof surrounding rock, and the maximum stress concentration coefficient is about 1.6

(4) To enhance the overall support strength of the roadway floor, a new "differentiated" combined support is proposed and field tested. It has been 13 months since the completion of main roadway repair in this section; no obvious deformation occurred, indicating that the support scheme effectively controls the deformation of deep soft rock roadway. It provides experience for roadway support in similar mines

Data Availability

The data used to support the findings of this research are included within the paper.

Conflicts of Interest

The authors declare that there are no conflicts of interest.

Acknowledgments

This work was supported by the National Natural Science Foundation of China (No. 51974317) and the Fundamental Research Funds for the Central Universities (2022YJSNY09).

References

[1] D. Y. Qian, N. Zhang, P. D. Jiang et al., "Stability of deep underground openings through large fault zones in argillaceous rock," *Sustainability*, vol. 9, no. 11, p. 2153, 2017.

[2] L. G. Wang, Y. L. Lu, Y. G. Huang, and H. Y. Sun, "Deep-shallow coupled bolt-grouting support technology for soft rock roadway in deep mine," *Journal of China University of Mining & Technology*, vol. 45, no. 1, pp. 11–18, 2016.

[3] H. J. Zhang, H. Y. Li, S. C. Li, J. W. Bai, H. A. O. Tingyu, and L. I. Hongwei, "Deformation mechanism of surrounding rock and support technology in deep soft rock roadway," *Journal of Mining & Safety Engineering*, vol. 32, no. 6, pp. 955–962, 2015.

[4] S. F. Liu, S. F. Lu, Z. J. Wan, H. W. Zhang, and K. K. Xing, "Numerical simulation of induced cutting in deep coal," *Royal Society Open Science*, vol. 6, no. 9, pp. 1–12, 2019.

[5] S. T. Ji, Z. Wang, and J. Karlovšek, "Analytical study of subcritical crack growth under mode I loading to estimate the roof durability in underground excavation," *International Journal of Mining Science and Technology*, vol. 32, no. 2, pp. 375–385, 2022.

[6] M. C. He, Y. Yuan, X. L. Wang, Z. Q. Wu, C. Liu, and Y. L. Jiang, "Control technology for large deformation of mesozoic compound soft rock in Xinjiang and its application," *Chinese Journal of Rock Mechanics and Engineering*, vol. 32, no. 3, pp. 434–441, 2013.

[7] A. A. Ilinets, A. A. Sidorento, and Y. G. Sirenko, "Computer modelling of a floor heave in coal mines," in *International Conference: Information Technologies in Business and Industry*, vol. 1333, 032028, 2019.

[8] J. C. Chang, D. Li, T. F. Xie, W. Shi, and K. He, "Deformation and failure characteristics and control technology of roadway surrounding rock in deep coal mines," *Geofluids*, vol. 2020, Article ID 8834347, 15 pages, 2020.

[9] D. Zhang, J. B. Bai, S. Yan, R. Wang, N. Meng, and G. Wang, "Investigation on the failure mechanism of weak floors in deep and high-stress roadway and the corresponding control technology," *Minerals*, vol. 11, no. 12, p. 1408, 2021.

[10] C. L. Wang, G. Y. Li, and A. S. Gao, "Optimal pre-conditioning and support designs of floor heave in deep roadways," *Geomechanics and Engineering*, vol. 14, no. 5, pp. 429–437, 2018.

[11] Y. B. Wu, J. H. Hu, X. Y. Zhang, Y. G. Qin, Z. B. Zhang, and X. C. Zhao, "Study on bearing capacity characteristics of steel structure support in soft rock roadway," *Energy Science & Engineering*, vol. 9, no. 12, pp. 2423–2433, 2021.

[12] X. H. Xu, F. L. He, X. B. Li, and W. R. He, "Research on mechanism and control of asymmetric deformation of gob side coal roadway with fully mechanized caving mining," *Engineering Failure Analysis*, vol. 120, article 105097, 2021.

[13] L. Shi, H. D. Zhang, and P. Wang, "Research on key technologies of floor heave control in soft rock roadway," *Advances in Civil Engineering*, vol. 2020, Article ID 8857873, 13 pages, 2020.

[14] W. R. He, F. L. He, K. Zhang, and Z. H. Xu, "Diffusion mechanism and parameter optimization in the process of grouting reinforcement of drenching and soft roadway," *Journal of Mining Science and Technology*, vol. 4, no. 3, pp. 221–229, 2019.

[15] Q. Wang, B. Jiang, R. Pan et al., "Failure mechanism of surrounding rock with high stress and confined concrete support system," *International Journal of Rock Mechanics and Mining Sciences*, vol. 102, pp. 89–100, 2018.

[16] S. Mo, H. L. Ramandi, J. Oh et al., "A new coal mine floor rating system and its application to assess the potential of floor heave," *International Journal of Rock Mechanics and Mining Sciences*, vol. 128, article 104241, 2020.

[17] M. Wang, D. J. Zheng, K. W. Wang, and W. F. Li, "Strain energy analysis of floor heave in longwall gateroads," *Royal Society Open Science*, vol. 37, no. 8, 2018.

[18] C. J. Hou, "Effective approach and basic frame-work of surrounding rocks control in deep roadway," *Journal of China University of Mining & Technology*, vol. 46, no. 3, pp. 467–473, 2017.

[19] D. M. Guo, X. C. Kang, Z. Y. Lu, and Q. Y. Chen, "Flexural floor heave mechanism and floor corner piles control technology in soft rock roadway," *Journal of Mining Science and Technology*, vol. 5, no. 6, pp. 536–545, 2021.

[20] H. P. Kang, *Mechanism and Control of Floor Heave in Soft Rock Roadway*, China Coal Industry Press, Beijing, CHINA, 1993.

[21] J. Yang, K. F. Zhou, Y. Cheng, Y. Gao, Q. Wei, and Y. Hu, "Mechanism and control of roadway floor heave in the Paleogene soft rock surroundings," *Geotechnical and Geological Engineering*, vol. 37, no. 6, pp. 5167–5185, 2019.

[22] L. Z. Xu and S. J. Wei, "Control technology and simulation study of floor heave in high stress soft rock roadway," *Geotechnical and Geological Engineering*, vol. 38, no. 4, pp. 4045–4058, 2020.

[23] Z. J. Wen, J. Y. Lu, Q. H. Xiao, and G. Y. Chen, "Failure mechanism of floor heave and supporting technology of soft rock roadway," *Journal of China Coal Society*, vol. 44, no. 7, pp. 1991–1999, 2019.

[24] Z. Q. Wang, P. Wang, W. Y. Lv, and L. Shi, "Mechanism and control of asymmetric floor heave in gob-side entry," *Journal of Mining & Safety Engineering*, vol. 38, no. 2, pp. 215–226, 2021.

[25] J. Sun, "Numerical simulation of grooving method for floor heave control in soft rock roadway," *International Journal of Mining Science and Technology*, vol. 21, no. 1, pp. 49–56, 2011.

[26] A. Chen, Q. Ma, and X. S. Liu, "Evaluation method of floor heave damage degree and a case study in Zaoquan coal mine, China," *Shock and Vibration*, vol. 2021, Article ID 2294894, 10 pages, 2021.

[27] X. M. Sun, F. Chen, M. C. He, W. L. Gong, H. C. Xu, and H. Lu, "Physical modeling of floor heave for the deep-buried roadway excavated in ten degree inclined strata using infrared thermal imaging technology," *Tunnelling and Underground Space Technology*, vol. 63, pp. 228–243, 2017.

[28] H. Cheng, H. B. Zhao, J. F. Xu, F. Y. Qin, Y. X. Zhang, and L. F. Hu, "Study on floor heave mechanism and control technology of roadway based on slip line field theory," *Journal of Mining Science and Technology*, vol. 6, no. 3, pp. 314–322, 2021.

[29] H. P. Kang, M. J. Fan, F. Q. Gao, and H. Zhang, "Deformation and support of rock roadway at depth more than 1000 meters," *Chinese Journal of Rock Mechanics and Engineering*, vol. 34, no. 11, pp. 2227–2240, 2015.

[30] K. Himammoto, T. Kawagoe, and K. Yashiro, "Estimation of floor heave mechanism of rock tunnels focused on the change in water content," *Journal of Japan Society of Civil Engineers, Ser. F1 (Tunnel Engineering)*, vol. 76, no. 1, pp. 34–48, 2020.

[31] S. T. Ji, H. Hu, and J. Karlovšek, "Application of superposition method to study the mechanical behaviour of overlying strata in longwall mining," *International Journal of Rock Mechanics and Mining Sciences*, vol. 146, article 104874, 2021.

[32] Z. Y. Chen, J. X. Zhou, and H. J. Wang, *Soil Mechanics*, Tsinghua University Press, Beijing, CHINA, 1992.

[33] Q. S. Huang and J. L. Cheng, "Research on analytic calculation model for mining induced stress in multilayered floor rock," *Journal of Mining Science and Technology*, vol. 2, no. 6, pp. 559–565, 2017.